



Investigation on strong vertical permeability and micro-pore characteristics of Jinan red clay using X-ray micro-tomography

Hao Cai¹ · Qi Zhang¹ · Guanlin Ye¹ · Linhai Lu^{2,3,4} · Chaojun Wu^{3,4} · Fang Ji^{3,4}

Received: 2 February 2022 / Accepted: 12 February 2023 / Published online: 25 February 2023
© The Author(s), under exclusive licence to Springer-Verlag GmbH Germany, part of Springer Nature 2023

Abstract

Due to the peculiarity of the spring domain strata in Jinan, the phenomenon of serious water seepage appears in the process of excavation. The macro permeability of soil is closely correlated with its microstructure. In this study, using the X-ray micro-tomography (micro-CT) system and a self-designed soil seepage device, the internal pore structure of Jinan red clay and the water flow inside the sample under different seepage stages were observed. The microstructure of water phase and air phase in the sample was segmented by the watershed algorithm. Calculation and comparison of pore and throat size distributions and coordination number (CN) at different seepage stages were conducted by establishing pore network model (PNM). Meanwhile, the seepage experiment simulations were conducted based on the 3D pore structure of red clay. The results show that the preferentially flow of Jinan red clay is obvious due to the existence of the vertically developed macropore channel. The fine particles (mainly silt particles) are washed away during seepage, thereby expanding the pore channels. The maximum pore radius and pore connectivity have important influence on seepage characteristics of Jinan red clay, but the correlation between porosity is small.

Keywords X-ray micro-tomography · Red clay · Soil permeability · Three-dimensional pore network · Seepage simulation

Introduction

During the construction of Jinan rail transit, engineers have encountered difficulties in excavation dewatering. Even with the construction of waterproof curtain, the dewatering problem of the foundation pit was still not completely solved, which brings great risks to the construction. At the construction site, the water seepage is very likely to occur at the bottom of the excavation, where many visible pore channels exist. It is thus speculated that the long-term upward seepage of groundwater leads to the existence of vertical seepage

channels in the Jinan red clay stratum, and thus reveals a strong vertical permeability.

Soil seepage is affected by many factors, including soil particle size (Zhang et al. 2018; Liu et al. 2021) mineral composition (Chen et al. 2022), soil pore structure (Luo et al. 2010), dynamic viscosity of pore fluid (Nguyen et al. 2013) and hydromechanical conditions (Chang and Zhang 2013). Numerous studies conducted before has focused on the seepage characteristics of clay (Miller and Low 1963; Rolfe and Aylmore 1977; Huang and Laften 1996). Boynton and Daniel (1985) performed the permeability tests on compacted clay to study the effects of hydraulic anisotropy, diameter of test specimens, storage time, and desiccation cracking. Liu and Birkholzer (2012) proposed a new relationship between water flux and hydraulic gradient to capture the non-Darcian flow behaviour of clay media.

Most of the mentioned studies on seepage characteristics of clay are from macroscopic field. As a non-destructive 3D reconstruction technology, X-ray micro-tomography (micro-CT) has been widely used in geotechnical engineering in recent years (Naveed et al. 2013; Taylor et al. 2015; Chen et al. 2021; Lyu et al. 2021). Many studies using micro-CT focus on the microscopic seepage characteristics of porous

✉ Qi Zhang
zhangqi33@sjtu.edu.cn

¹ State Key Laboratory of Ocean Engineering, Department of Civil Engineering, Shanghai Jiao Tong University, Shanghai, China

² Department of Transportation, Beijing Jiao Tong University, Beijing, China

³ Jinan Rail Transit Group Co., Ltd, Jinan, China

⁴ Jinan Transportation Development Investment Co., Ltd, Jinan, China

media, including observation of internal flow (Koestel and Larsbo 2014; Nguyen et al. 2019) and pore-scale flow modelling and simulation based on the micro-CT results (Wei et al. 2019). However, most of the above studies are focused on sand or rock, the study on microscopic seepage characteristics of clay is still limited.

In this study, the seepage experiment combined with X-ray micro-tomography was designed to obtain the micro-pore structure of Jinan red clay and visualize the seepage path of water. Meanwhile, the seepage experiment simulations were conducted based on the 3D structure of Jinan red clay. The hydraulic parameters that influence soil seepage characteristics most and the reasons for the pressing groundwater problem were identified. The reasons why Jinan red clay has strong vertical permeability were analyzed, and the scientific issues extended from the groundwater seepage problem were also discussed.

Engineering background and geological conditions

Jinan is a famous city in China also widely known as “Spring City”. The Quaternary sedimentary layer in Jinan is mainly composed of clay and silty clay, but shows high vertical permeability. The topography of Jinan is southern high and northern low-lying. The elevation of groundwater level in the southern mountainous area is about 100–137 m, which changes with atmospheric precipitation change. The elevation of groundwater level in Jinan city is 25–30 m. After atmospheric precipitation, surface water seeps into the ground and flows spontaneously from south to north. Figure 1 shows the schematic diagram of the formation of Jinan spring group. The stratum in the northern part of Jinan consists of Yanshanian intrusive rock, which is hard and

impermeable. The groundwater is blocked here, converging from horizontal movement to vertical upward movement. A large amount of groundwater passes through karst fissures and forms gushing springs.

The geological profile near the Peijiaying Metro Station is shown in Fig. 2. The red line is the boundary line between different soil layers, and the number represents the stratigraphic sequence number. The soil layer of the site is unevenly distributed, and the thickness of the filling layer is about 0.5–4.3 m. Loess is locally distributed under the filling layer. The elevation from 25.92 to – 6.18 m is the Quaternary silty clay and clay layer, which includes the typical high permeability Jinan red clay layer. The elevation from – 6.18 m to – 29.58 m is mainly gravel and silty clay containing gravel. The underlying bedrock of the site consists of diorite and limestone.

The stratum between permeable stratum and Ordovician limestone are mainly composed of high permeable gravel layer and completely weathered diorite layer, due to which the permeable stratum is directly recharged by the underlying limestone fissure confined water. The underlying Ordovician limestone layer 19 contains abundant karst water, which is attributed as aquifer, resulting in a high groundwater level, and the water inflow during the excavation of Peijiaying Metro Station is significantly greater than other areas. According to the field pumping test results, the average permeability coefficient of 9_1 to 14_1 silty clay layer is 1.42×10^{-5} – 1.41×10^{-4} m/s, with 5.3×10^{-7} m/s for 16 clay layer, and 4.02×10^{-4} – 4.67×10^{-4} m/s for 17 gravel layer and 18 diorite layer. The soil samples were obtained from the typical permeable red clay stratum–layer 10 silty clay, which has the highest permeability coefficient of 1.41×10^{-4} m/s among all the clay and silty clay layers. Undisturbed samples were obtained using thin-walled tube sampling with PVC pipes. These sharp-edged pipes

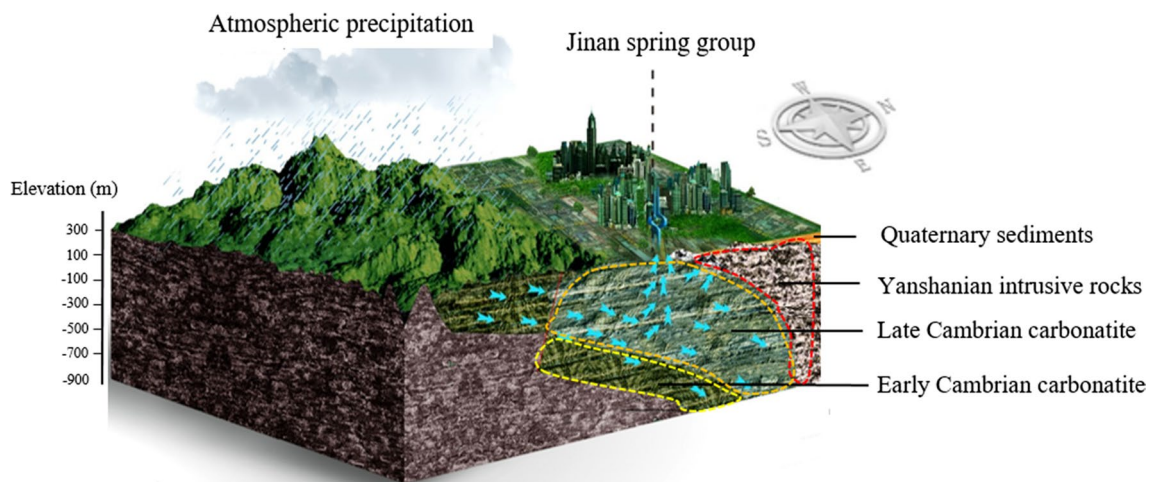


Fig. 1 Formation of Jinan spring group

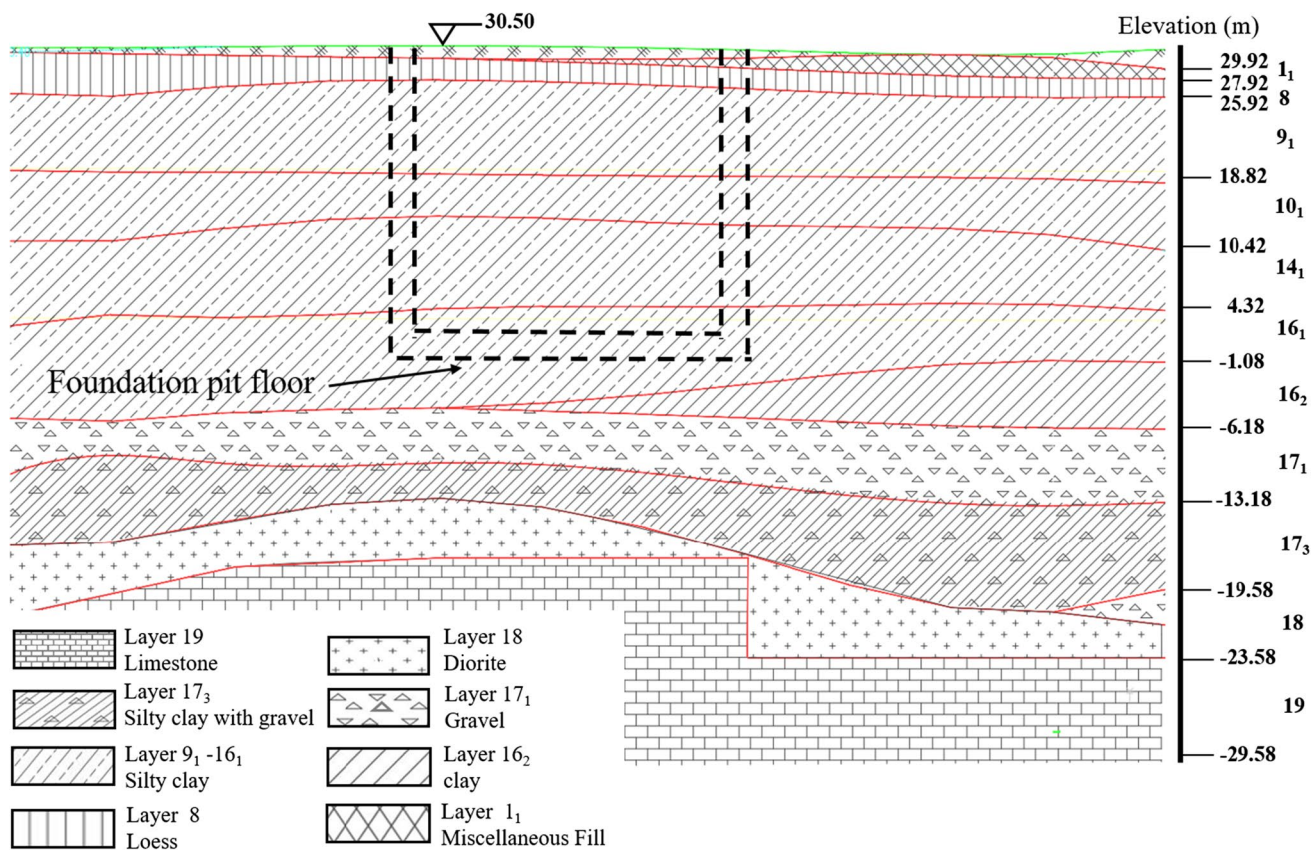


Fig. 2 Stratum map of permeable foundation pit in Jinan

can avoid disturbance on the sample as much as possible for laboratory testing. The physical properties and the mineral composition are determined by X-ray diffraction (XRD) and is listed in Table 1. It is noted that Jinan red clay has a higher organic carbon content (2% in average) compared to silty clay with similar particle composition (Koestel and Larsbo 2014; Larsbo et al. 2014), indicating that there may be carbonized plant roots during the deposition process. Therefore, it can be inferred that the red clay layer in Jinan has formed many vertically developed pores under the action of long-term vertical seepage, and exists macropore channels, resulting in the high permeability of these layers of soil.

To verify the conjecture, the seepage experiment of Jinan red clay was designed based on X-ray micro-tomography to

obtain the micro-pore structure of Jinan red clay and observe seepage path of water in the soil sample.

Testing procedure and technology

Testing procedure

Three red clay samples from different parts of intact soil column are trimmed into a cylinder with diameter of 5 cm and height of 10 cm (Fig. 3) followed by scanning of three intact samples by micro-CT to obtain the pore characteristics of Jinan red clay at different depths. The first micro-CT scanning experiment for top sample (T1) has lower spatial resolution to get a wider scanning field. The middle (M1)

Table 1 Physical properties and mineral composition of Jinan red clay

Physical properties					Mineral composition (%)			
Natural density (g/cm ³)	Initial void ratio	Natural water content (w _n %)	Hydraulic conductivity (×10 ⁻⁴ m/s)	Organic carbon content (%)	Quartz	Illite	Albite	Montmorillonite
1.99	0.701	25.40	1.41	12.18	42.4	40.2	16.8	0.6

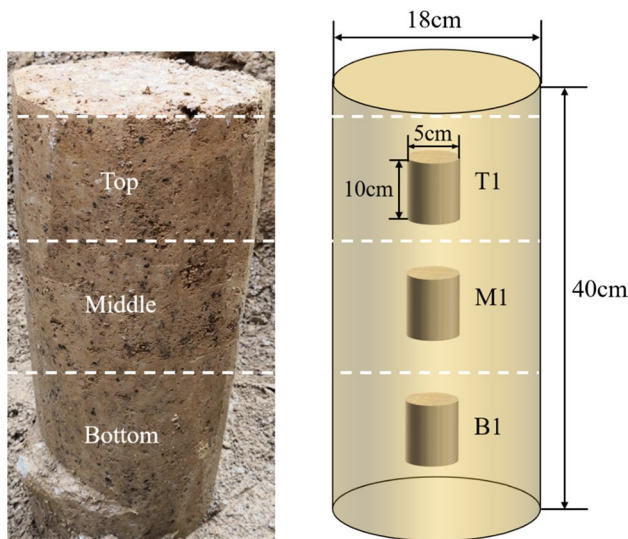


Fig. 3 Intact Jinan red clay column and the sample positions

and bottom (B1) samples were scanned with a higher spatial resolution to observe the internal pore morphology of red clay more distinctly, and the middle sample (M1) was adopted in the seepage experiment.

Figure 4 shows the schematic figure and photo of seepage experiment for Jinan red clay. The seepage apparatus made of PMMA is designed as two parts, the main body and the base, which are connected with each other through screw threads. First, the sample is trimmed into a cylinder with diameter of 5 cm and height of 10 cm. Then, the sample is put into the PMMA container with silicone grease on each side, and the main body and the base are screwed by threads. The prepared gypsum liquid is dropped into the gap between the sample and the side wall of the container to prevent water from flowing up from the gap. Finally, two sealing hoops are added at the bottom and top of the apparatus body to ensure that the container is sealed. A channel is set up in the base and connected with a plunger pump (GDS Instruments Co., UK) for external water supply to simulate the seepage of water from bottom to top in the soil. The seepage apparatus is fixed on the rotation stage between the X-ray source and the detector as shown in Fig. 5, which enables the seepage apparatus to be rotated by plus or minus 180° during scanning.

The whole seepage experiment based on micro-CT is divided into three stages: (1) intact sample (M1); (2) Intermediate stage of seepage experiment; (3) End stage of seepage experiment. The time of water flowing from the bottom to the top of the sample is determined by a large number of preliminary experiments, and the approximate time from the water flow to the middle of the scanning range is estimated. In this seepage experiment, a water supply pressure of 10 kPa with a flow rate of $4.88 \times 10^{-7} \text{ m}^3/\text{s}$ was provided

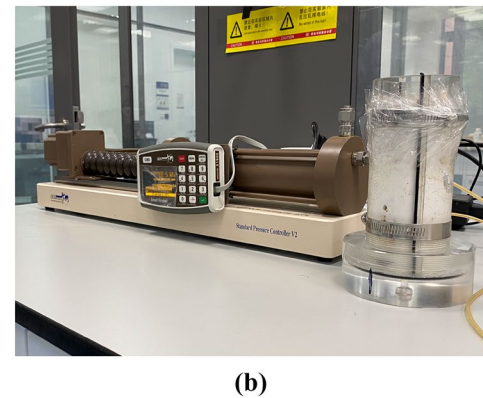
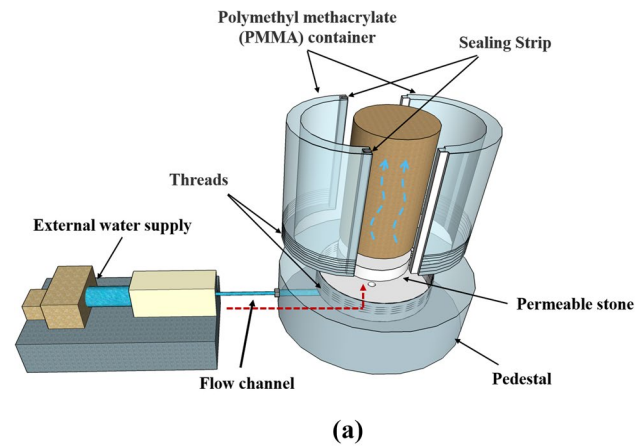


Fig. 4 **a** Schematic figure, and **b** apparatuses of the seepage experiment

by a plunger pump (GDS Instruments Co., UK). Based on the measured discharge flow rate ($1.47 \times 10^{-7} \text{ m}^3/\text{s}$) and the controlled hydraulic gradient (10), the permeability of Jinan red clay can also be obtained as $7.51 \times 10^{-6} \text{ m/s}$. The time of water supply of the intermediate stage and end stage was 6 min and 35 min, respectively. The apparatus was moved

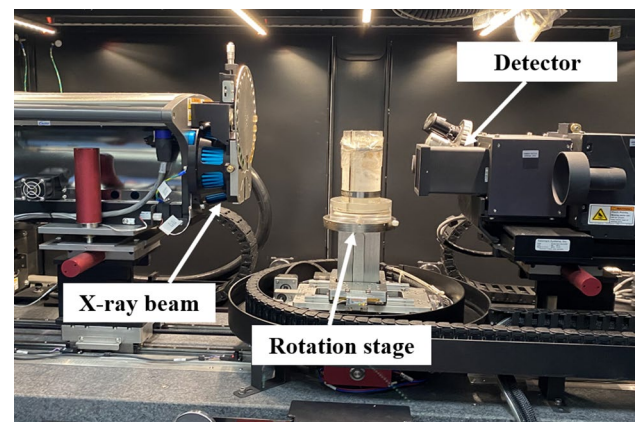


Fig. 5 X-ray micro-tomography setup and seepage apparatus

to the CT scanning room immediately after the water supply was finished. The water injected into the sample was added with iohexol, a water-soluble X-ray contrast medium, to make it easier to distinguish water and air in soil.

The micro-CT apparatus used in this study is the Zeiss Xradia 520 Versa in Instrumental Analysis Center of Shanghai Jiao Tong University. The micro-CT system was operated at a voltage of 140 kV and a current of 71.6 μ A and the X-ray power was 10 W during the scanning process. The partial CT scan with cylinder scanning field of a diameter of 2.5 cm and a height of 2.5 cm in the middle of the sample is used to avoid the boundary effects. The specification of the X-ray CT system and the parameters used in this study are shown in Table 2.

Image analysis

Figure 6 illustrates the image processing procedure on a horizontal slice of the intact sample. The 16-bit slices of

Table 2 Specification of the X-ray CT system

X-ray source	
Maximum voltage	160 kV
Minimum voltage	30 kV
Maximum current	1 mA
Maximum spatial resolution	700 nm
Image intensifier	
Size of detector	9 inches
CCD pixel size	20,482
CT image	
Voxel size (um)	T1: 48.82×49.3 M1: 25.02×24.6 B1: 26.12×26.3
Exposure time (s)	
	T1: 2 M1: 3.5 B1: 3.5
Scanning method	
	Partial scan

CT images are first converted into 8-bit gray-scale images by software Image J followed by application of a 3D median filter to remove the random noise. Following this process, the filtered image is segmented by “Moments” automatic threshold method in Image J. After that, the raw CT image is converted into filtered binary image shown in Fig. 6d. For the sample after water penetration, the air phase and water phase of Jinan clay were segmented by a region-based watershed algorithm (Thermo Scientific Avizo Software User's Guide 2015).

Validation of watershed segmentation method

The watershed segmentation method has been used in many researches (Wang et al. 2019; Zhou and Xiao 2019; Yu et al. 2020). To verify the effectiveness and accuracy of watershed segmentation method, an experiment is first carried out based on micro-CT in this study.

The red clay sample was trimmed into a cube with the size of 3.8 cm×3.8 cm×4.2 cm (length×width×height). A hole was drilled from the top surface of the sample, which filled with a PMMA (Polymethylmethacrylate) tube. The PMMA tube was filled with a certain height of water, as shown in Fig. 7. Then, the sample was scanned by micro-CT to visualize the air, water and soil particles in red clay.

Figure 8 shows the results of typical horizontal section of the sample. Water, PMMA tube and the air are depicted

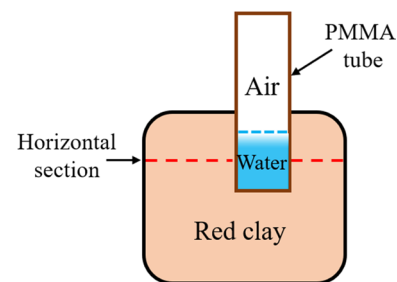


Fig. 7 Schematic diagram of the sample

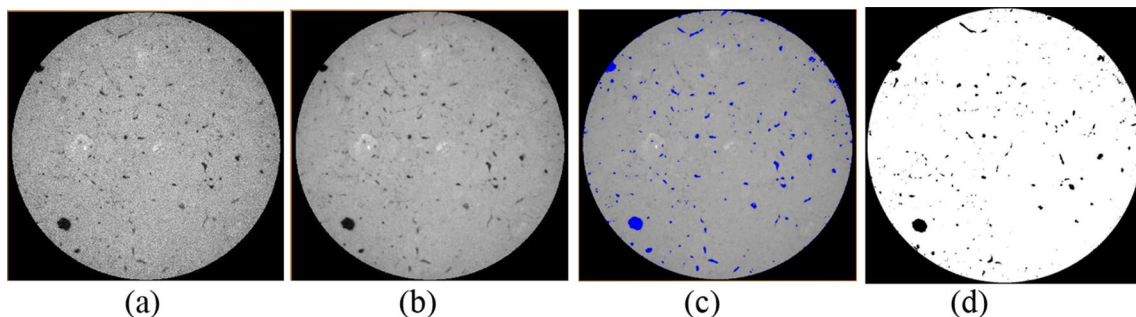


Fig. 6 Illustration of image processing procedure on a horizontal slice of the sample before seepage experiment: **a** Raw picture, **b** After applying 3D median filter, **c** During threshold segmentation, and **d** Final segmented image

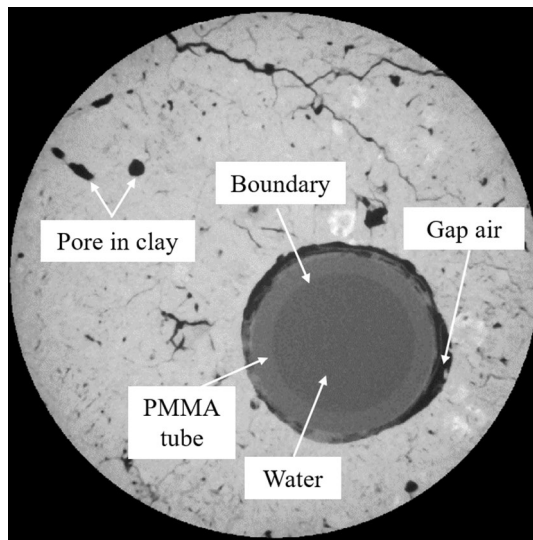
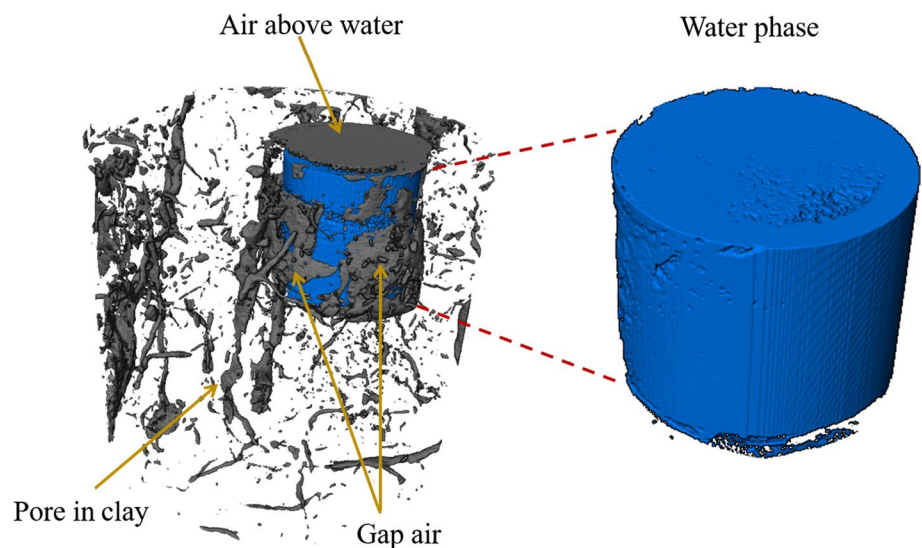


Fig. 8 Typical horizontal cross section of the sample

in different color due to different density. The boundaries between the water and the PMMA tube, PMMA tube and air are distinguishable. Therefore, the watershed segmentation method of segmenting water, soil and pores is applicable. Based on the seed markers and the gradient image, the watershed expansion of the seed markers towards boundary is completed, and the air phase and water phase in soil are successfully segmented and extracted, as shown in Fig. 9. The effectiveness of the watershed segmentation is validated.

Fig. 9 Three-dimensional structure of air and water in the sample



Results and discussion

Pore structure of intact Jinan red clay

The 3D pore space and soil matrix of intact Jinan red clay sample at different depths were reconstructed and segmented via stacking 1020 binary images using the image processing software, Avizo (FEI Co., USA). The pore structure of intact Jinan red clay sample at different depths are shown in Fig. 10. It should be noted that the sample T1 has a wider scanning field with lower spatial resolution, thus the pore structure looks smaller than that of the other two samples. It is noticed that the pore structure of Jinan red clay at different depths mainly developed vertically with good connectivity. There are vertical pore channels with large pore diameter in all three samples.

Comparison between different stages of seepage experiment with CT scanning

The density of objects is linearly related to the CT value. In CT images, regions of higher density are indicated by lighter color, such as white or light gray, while the lower density regions are denoted by dark color, such as black. The clay particles appear as light gray and the pores filled with water and unfilled pores appear as light black and black, respectively.

Figure 11a–c shows the vertical slices of 3D reconstruction of the sample under three stages. The difference between Fig. 11a, b is caused by the deviation of the scanning area. At the end of each soil scanning stage, the soil sample needs to be taken out of the scanning chamber for the seepage test, and then the next scanning stage is carried out. This resulted in a deviation of about 2% between the

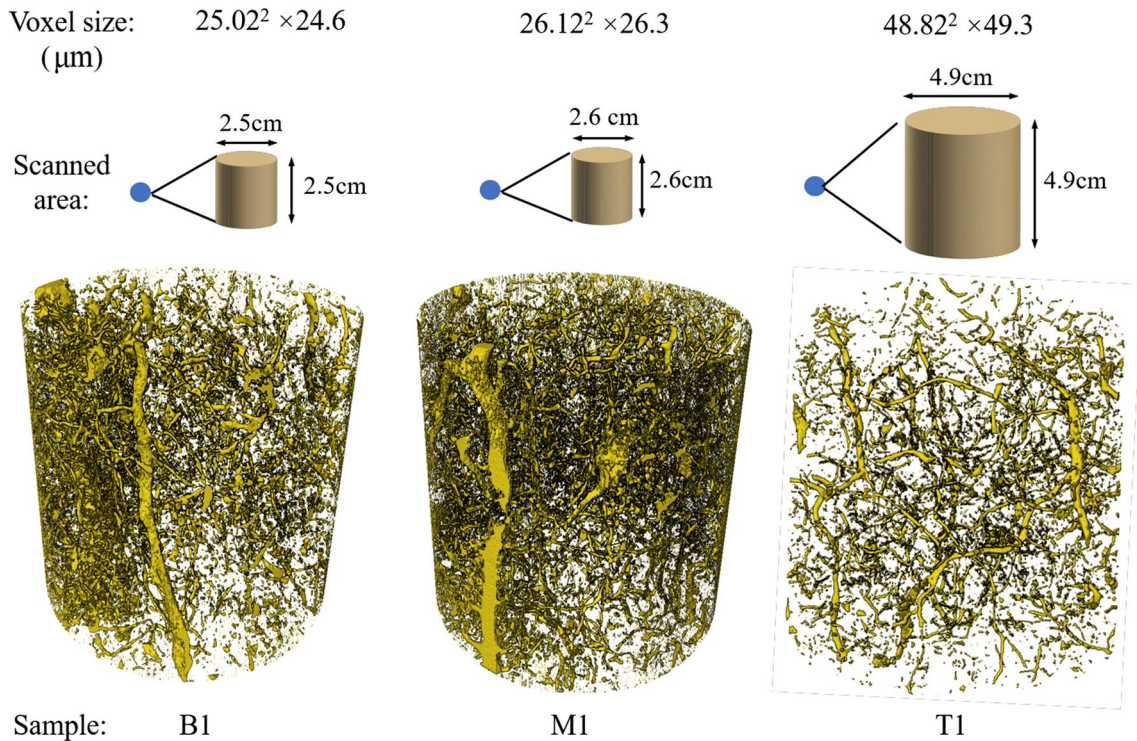


Fig. 10 Pore structure of intact Jinan red clay sample

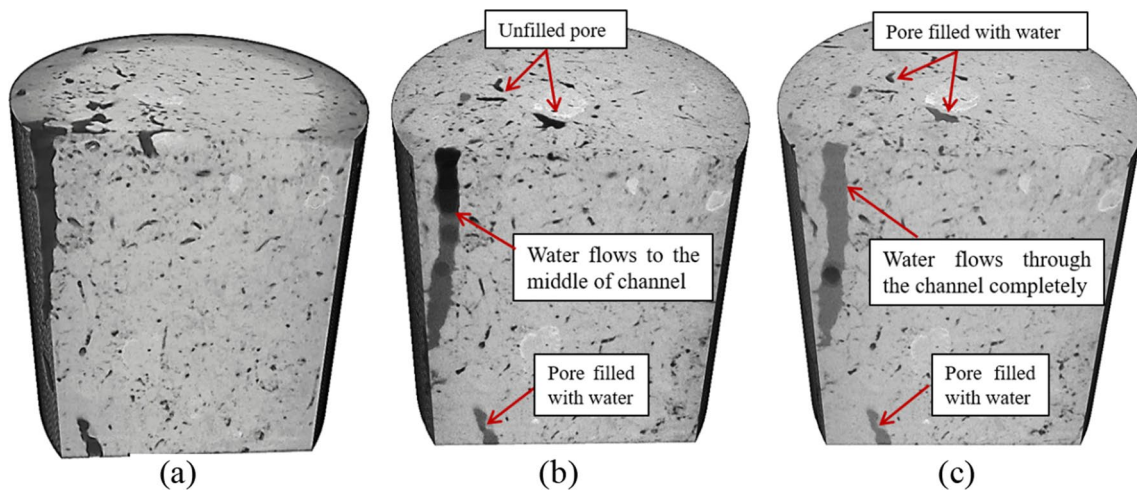


Fig. 11 Vertical slices in the YZ plane of 3D reconstruction of the sample under different seepage stages: **a** intact sample, **b** intermediate stage of seepage experiment, and **c** end stage of seepage experiment

scanned areas of the first and second stages. However, it is still possible to perform a comparative analysis of the different seepage stages with some representative pore structures. In addition, the difference has little impact on the preferential flow visualization and other issues concerned in this study. It can be observed that there is a connected pore channel in the left side of the sample in Fig. 11a. With the progress of water supply, the water flowed along the

channel in the sample. The water flowed to the middle of the seepage channel in the intermediate stage of seepage experiment and completely passed through the seepage channel at the end stage of seepage experiment, as shown in Fig. 11b, c. The “Thickness Map” function in Avizo was applied in the pore space of Jinan red clay under different seepage stages (Fig. 12). Applying the Thickness Map algorithm on a binary image gives a gray level image, where each voxel

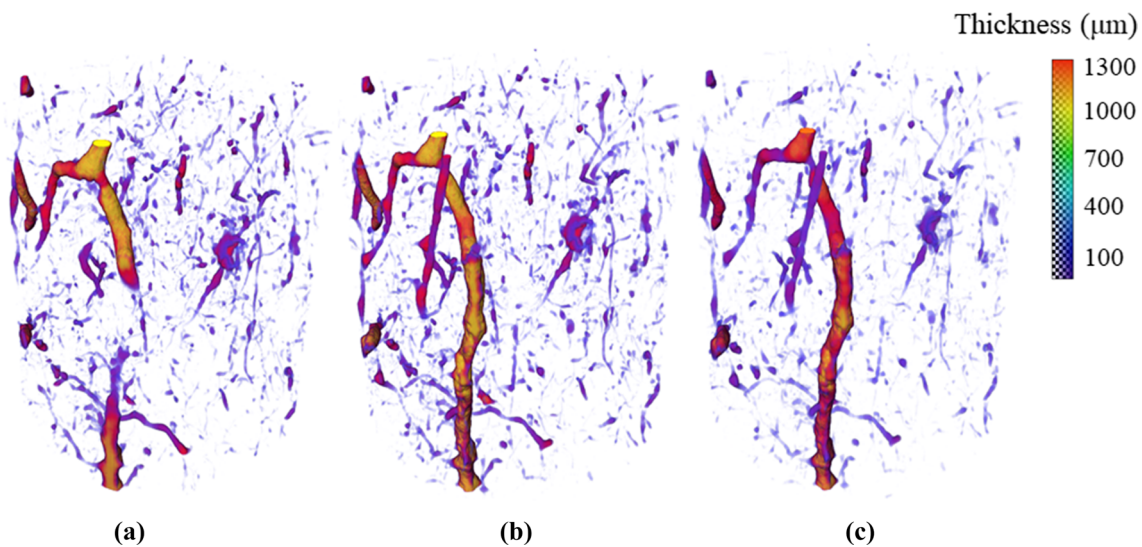


Fig. 12 Thickness of pore structure of the sample at different stages: **a** intact sample, **b** intermediate stage of seepage experiment, and **c** end stage of seepage experiment

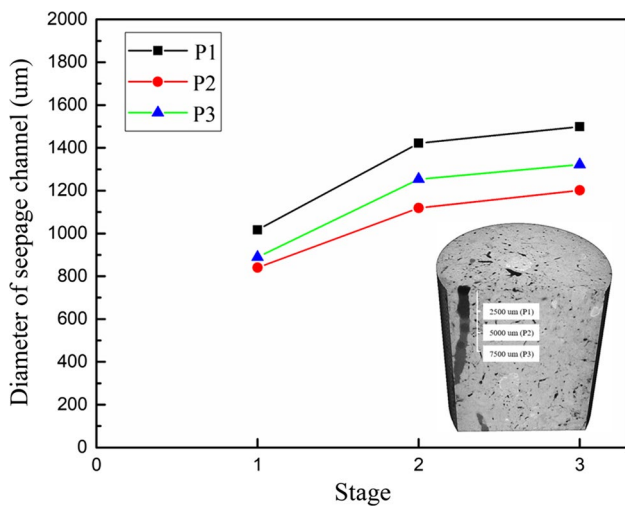


Fig. 13 Diameter variation of seepage channel at different positions under three stages

intensity represents the minimal distance in voxels from the object boundary (Avizo Software 9 User’s Guide). Meanwhile, the diameter variation of the seepage channel at different positions under three stages were determined by the “Measure” function in Avizo based on the 3D pore structure (Fig. 13). Three points with different distances from the top of the seepage channel were selected, including 2500 µm, 5000 µm, and 7500 µm. As can be seen, the thickness of the macro-pore on the left was observed to increase with the progress of seepage experiment, especially in the initial stage of water supply. The result indicates that the seepage channel expands during the seepage experiment.

The watershed segmentation was applied to separate and extract air phase and water phase from the sample under different seepage stages. Subsequently, a volume rendering module was applied to observe the 3D structure of air and water phase in soil (Fig. 14). It can be concluded that when water flows through the clay, it will flow preferentially along the existing connected pore channels of clay from the comparison between three stages, as shown in Figs. 11 and 14.

During the seepage experiment of Jinan red clay, some soil particles were washed out from the pore channel with the clay matrix stay intact, these particles were collected carefully and dried using an oven. Then, the Laser particle size analyser (LPSA) was used to obtain the composition of these particles. The hydrodynamic dragging force was estimated as 6.23 Pa based on the equation proposed by Reddi et al. (2000):

$$\tau = \frac{\Delta P}{\Delta L} \sqrt{\frac{2K}{n}} \tag{1}$$

$$K = k \frac{\eta}{\gamma_w} \tag{2}$$

where $\frac{\Delta P}{\Delta L}$ is the pressure gradients, K is the absolute permeability, n is the porosity of the soil sample, k is the hydraulic conductivity, η is the viscosity of the fluid, γ_w is the weight of the fluid.

The comparison of grain size distribution is shown in Fig. 15. It is known that the intact Jinan red clay is mainly composed of 10% sand, 40% silt, and 50% clay. The soil particles washed out by water are mainly fine particles, including 80% silt particles and 20% clay particles, and

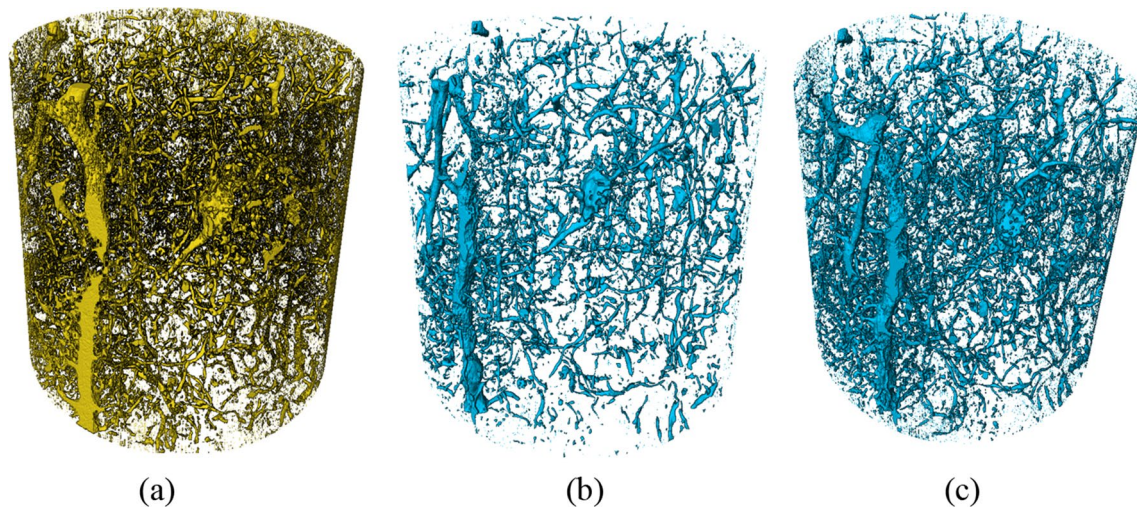


Fig. 14 Three-dimensional structure of air and water in sample at different stages based on watershed segmentation algorithm: **a** intact sample (Pore space), **b** intermediate stage of seepage experiment (Water), and **c** end stage of seepage experiment (Water)

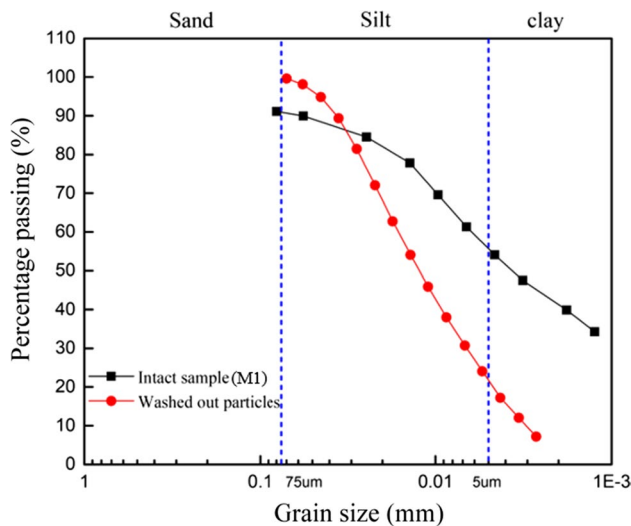


Fig. 15 Comparison of grain size distribution of intact Jinan red clay and washed out particles

there are basically no sand particles. The seepage experiments with different water supply pressures were conducted on the T1 and M1 sample to check the authenticity of the result. The pressures were increased from 20 to 40 kPa with the estimated hydrodynamic dragging force as 12.46 Pa and 24.92 Pa, respectively.

Figure 16 shows the comparison of grain size distribution of two intact samples and washed-out particles. With most of the silt particles and a small portion of the clay particles washed out, similar type of result was obtained. In addition, in the process of seepage experiment, only particles were found to be washed out by water from the seepage channels, while no soil particles were washed out in other parts of the

soil body, implying that washed-out particles mainly come from the pore walls, while the clay matrix stays intact.

The visualization results show that water flows preferentially along the macro-pore channel which in the space between the aggregates, resulting in the detachment of soil particles. Hence, it can be concluded that water flow preferentially along the existing connected pore channel of clay, during which the fine particles are washed away, thereby expanding the seepage channels. More discussion was presented in “Analysis of the micro-pore characteristics based on the establishment of Pore Network Model (PNM)”.

Analysis of the micro-pore characteristics based on the establishment of pore network model (PNM)

After the reconstruction of pore space, the Pore Network Model (PNM) was established (Fig. 17), with air phase for intact sample, air phase and water phase for samples at intermediate stage and end stage of seepage experiment. In the PNM, the algorithm divides the pore space into pore bodies and pore throats, which are represented by red spheres and grey sticks shown in Fig. 18, respectively. The true pore sizes were represented by the radius of sphere r_n (named EqRadius in Avizo, calculated for spheres with the same volume as an irregularly shaped pore body). The throats were modelled as cylinders using the contact area between two pore bodies, the stick thickness is the EqRadius of true throats and the throat length is represented by the distance between the pore centres along the direction of the pores. By generating the PNM, important macroscopic transport properties, including capillary pressure, relative permeability and residual saturation can be computed (Sakellariou et al. 2004; Zhao et al. 2019). Calculation and analysis of pore and throat

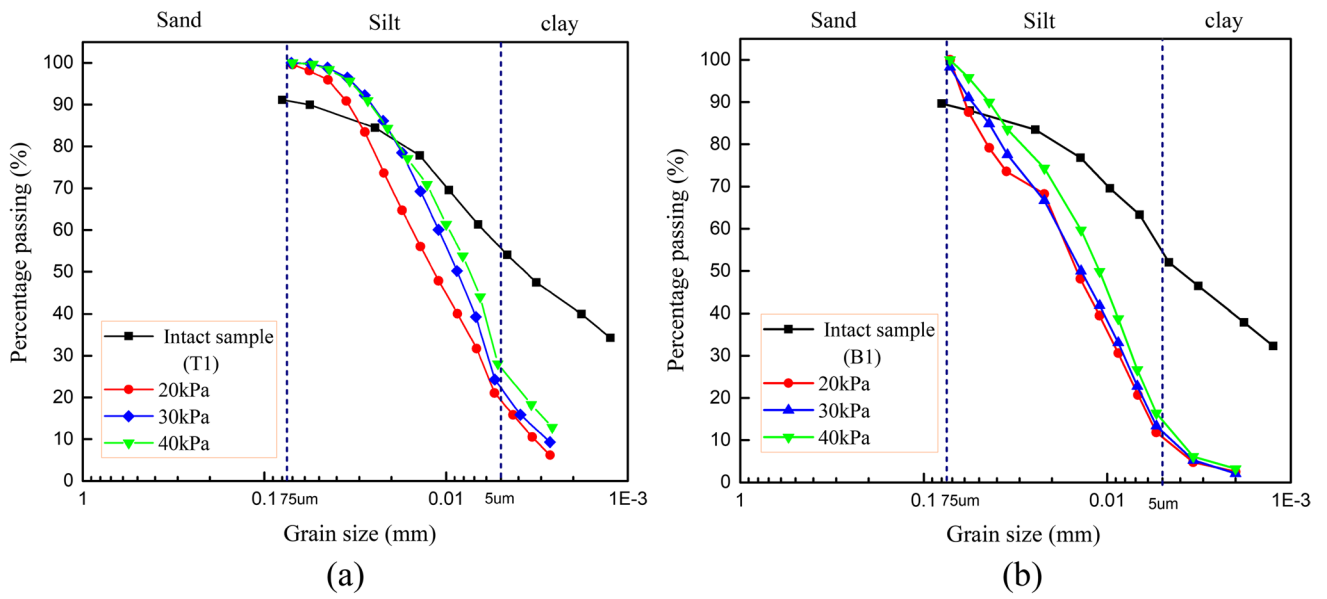


Fig. 16 Comparison of grain size distribution of intact Jinan red clay and washed out particles under different water supply pressures: **a** T1 sample, and **b** B1 sample

Fig. 17 Three-dimensional structure of pore space: **a** raw pore space structure and **b** pore network model (PNM)

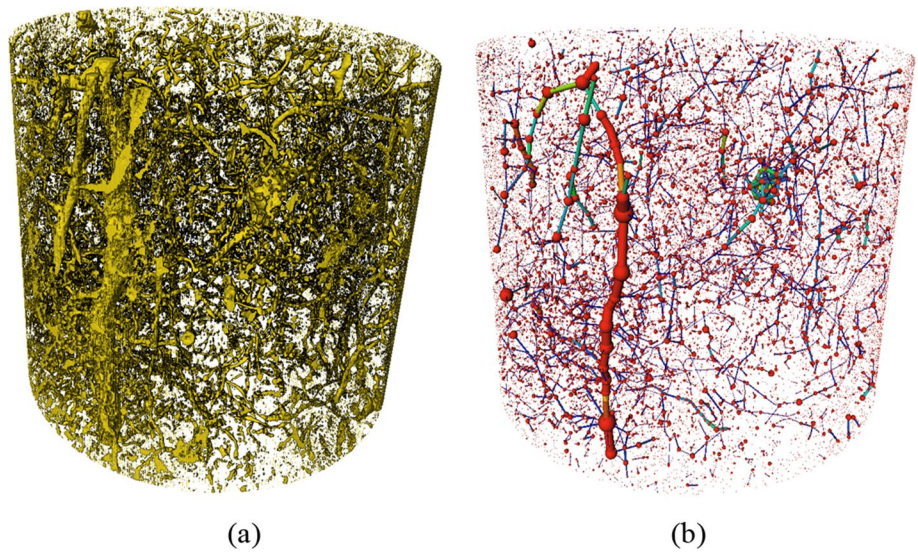
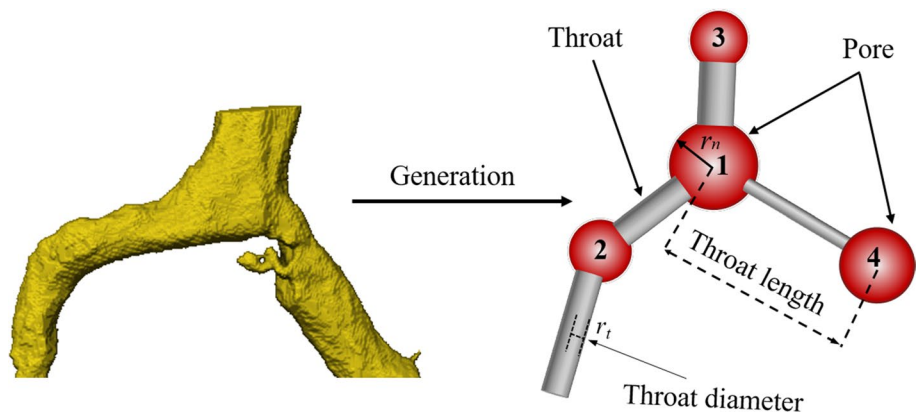


Fig. 18 Schematic diagram to generate PNM



size distributions at different seepage stages are conducted in this study. From Fig. 17, it is clear to see that the pores in intact Jinan red clay are mainly developed vertically and most of them are connected, indicating the good permeability of Jinan red clay in vertical direction. It can also be verified from the SEM image of Jinan red clay (Fig. 19), the soil particles in the vertical section are arranged more closely with less pores compared with the horizontal section.

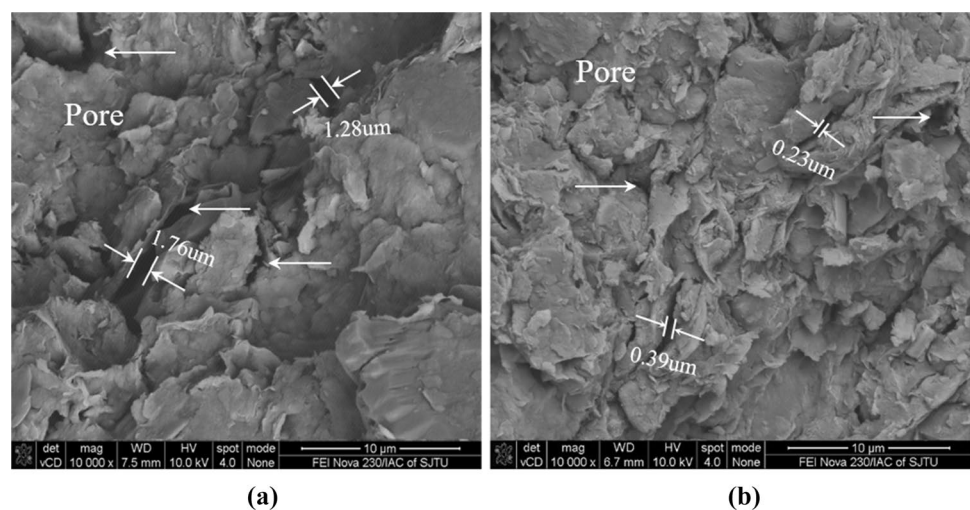
Figure 20 shows the pore and throat size distributions of Jinan red clay sample under three different stages of the whole experiment. “Count” represents the quantity of the pores and throats under a particular class. The results indicate Jinan red clay is mainly composed of small pores with pore EqRadius less than 100 μm . From the comparison of pore and throat size distribution in the three stages, we can illustrate that the number of pores and throats with large EqRadius is increasing with the progress of seepage experiment (Fig. 20a, c). In the stage 2 and stage 3, the pores with EqRadius larger than 200 μm increase by 11.5% and 18.9% in number, and the throats with EqRadius larger than 150 μm increase by 44.1% and 110.3% in number, respectively, which means the expansion of seepage channel. The distribution of throat length presented in Fig. 20b shows that throats with length larger than 500 μm increase by 1.3% and 3.7% in number, respectively. The result indicates that the distribution of pore throat length changes slightly during seepage experiment. It can be attributed that the pore structure of the soil has not been damaged in the initial stage of seepage, nor does it cause excessive migration of clay particles. This result is consistent with the comparison of grain size distribution shown in Figs. 15 and 16.

It is worth noticing that the expansion of macropore in Jinan clay is contrary to the results of the decrease of macropore size of compacted granular mixtures (Alonso et al. 2011) and silty loess (Zuo et al. 2020). The compacted granular mixtures used in the Alonso’s study were obtained

from Febex bentonite powder, which has over 90% montmorillonite content. So the aggregates in soil will expand and occupy the macropores when subjected to water infiltration. However, the Jinan red clay has low aggregates expanding potential, considering the low montmorillonite content (0.6%). What’s more, based on the conceptual model “Small Clay—Large Clay” proposed by Jefferson and Smalley (1995), the Jinan red clay is classified as “Large Clay”. At low clay contents (i.e., “Small Clay”), the soil behavior is predominantly frictional and the short-range bonds between quartz particles are produced. The short-range bonds, which tend to dominate in collapsing soil systems, can easily lose strength due to a slight deformation. Compared with “Small Clay”, the “Large Clay” has larger strain stiffness and strength due to the formation of long-range bonds (Ghadr and Assadi-Langroudi 2018). So the clay matrix tends to stay intact during the seepage experiment, instead of collapsing, so that the particles clog the pore space. Only particles on the pore wall were washed out, resulting the macropore channel expands slightly. The conceptual model also verifies the results of throat distribution among three seepage stages. In the study conducted by Zuo, the detached fine particles were also observed, but there was no further suffusion occurred, so that the macropores were occupied by detached particles.

Figure 21 shows the distribution of pore volume proportion and throat surface area proportion of the sample under three different stages of the whole experiment. The results show that the proportion of pore volume and throat surface area both increases for large pores (> 550 μm) and throats (> 450 μm). With the proportion of pore volume increases from 13.75 to 18.65%, the proportion of throat surface area increases from 8.21 to 19.44%. The increase of the proportion of large pores and throats results in the decrease of the proportion of small pores and throats. The results indicate that when water flows in the red clay, the macropore

Fig. 19 SEM image of Jinan red clay: **a** horizontal section and **b** vertical section



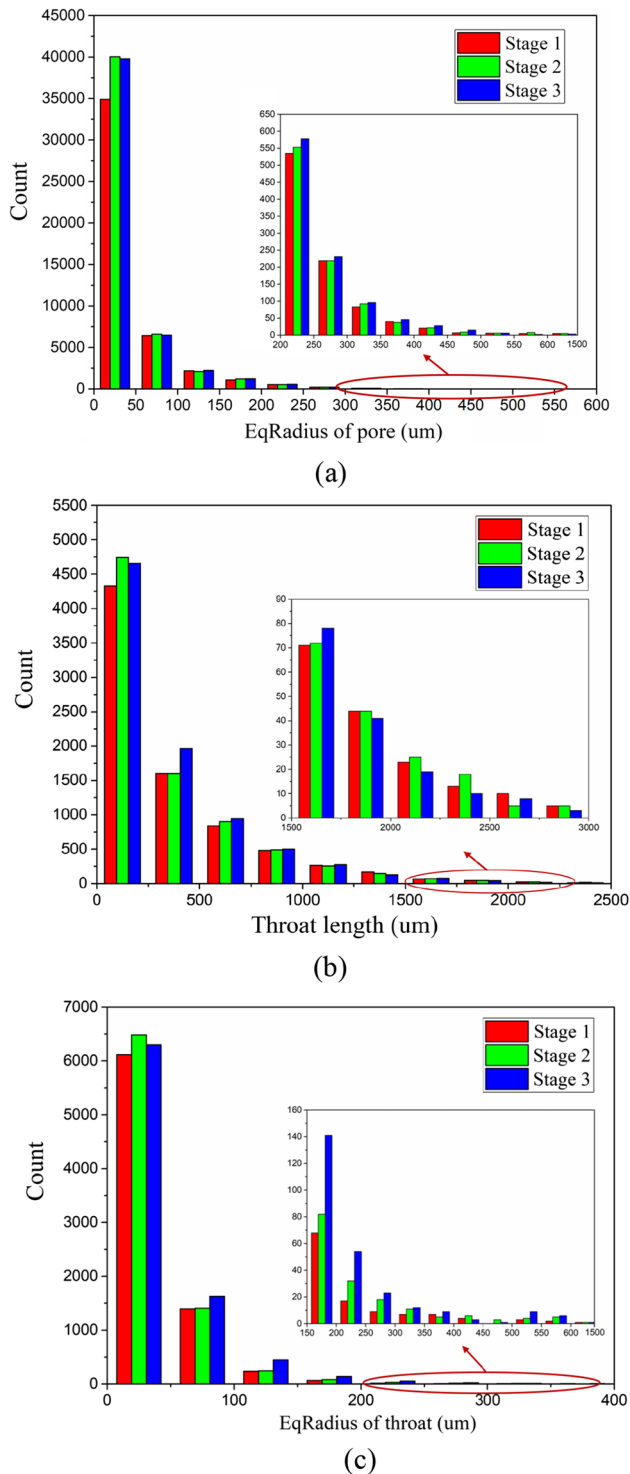


Fig. 20 Pore and throat size distributions of Jinan red clay under three different stages of the whole experiment: **a** pore EqRadius distribution, **b** throat length distribution, and **c** throat EqRadius distribution

channels have major influence on the seepage characteristics of red clay, while the influence of small pores can be ignored.

To analyse the pore connectivity of Jinan red clay, the coordination number (CN), which is defined as the number the throats connected to a given pore is introduced. For example, in Fig. 22, CN of pore 1 is three; pore 2: 2; pore 3 and 4: 1. The CN distribution with pore size of intact Jinan red clay and CN distribution variations under different seepage stages are shown in Figs. 22 and 23. It is known that the CN increase with the increasing pore EqRadius. Most pores had CN of 0, which are considered as isolated pores. With the progress of the seepage experiment, the total CN increases slightly and the average CN and the frequency of CN are basically unchanged, which also indicate the pore structure of the soil has not been damaged during seepage. The small pores are more likely with CN of 0, which are considered as isolated pores, and the macropores more likely have a good connectivity with greater CN. The results also show that the great importance of macropore on the soil seepage characteristics.

Three MIP experiments were also conducted on freeze-dried Jinan red clay samples to verify the conclusion. The PSD (Pore Size Distribution) curves are shown in Fig. 24. The Bimodal distribution is observed corresponding to the micro-pores with a dominant peak at 11.9 nm and the macropores with a dominant peak at 100 μm. The MIP results indicate that Jinan red clay has double-porosity characteristics, which relies on the existence of a micro-structural and a macro-structural domain (Della and Musso 2016). Based on the MIP results of Jinan red clay, the macro-porosity and micro-porosity were defined. The micro-pores correspond to intra-aggregate pores and have a size smaller than 3 μm; the macro-pores correspond to inter-aggregate pores and have a size greater than 3 μm. The micro- and macrostructural void ratios e_m and e_M obtained from MIP results are 0.659 and 0.165, respectively. The results also confirm that the small pores within the aggregates have little effect on the seepage characteristics of Jinan red clay, even though they account for a relatively high percentage. On the contrary, the macro-pores between the aggregates, which form preferential seepage channels, have major influence on the seepage characteristics of red clay.

Seepage experiment with X-ray computed tomography shows that under the influence of long-term vertical seepage, the pores in the undisturbed Jinan red clay are mainly developed vertically and most of them are connected, resulting in the good permeability of Jinan red clay in vertical direction. Due to the particularity of Jinan spring area stratum, the permeable stratum is directly recharged by the underlying Ordovician limestone layer, which contains abundant karst water. Therefore, during the excavation in areas such as Pei-jiaying Metro Station, serious excavation seepage problems have occurred even if waterproof curtains are installed. In this case, in addition to setting up waterproof curtain, it is also necessary to set up enough pumping wells or deep-well

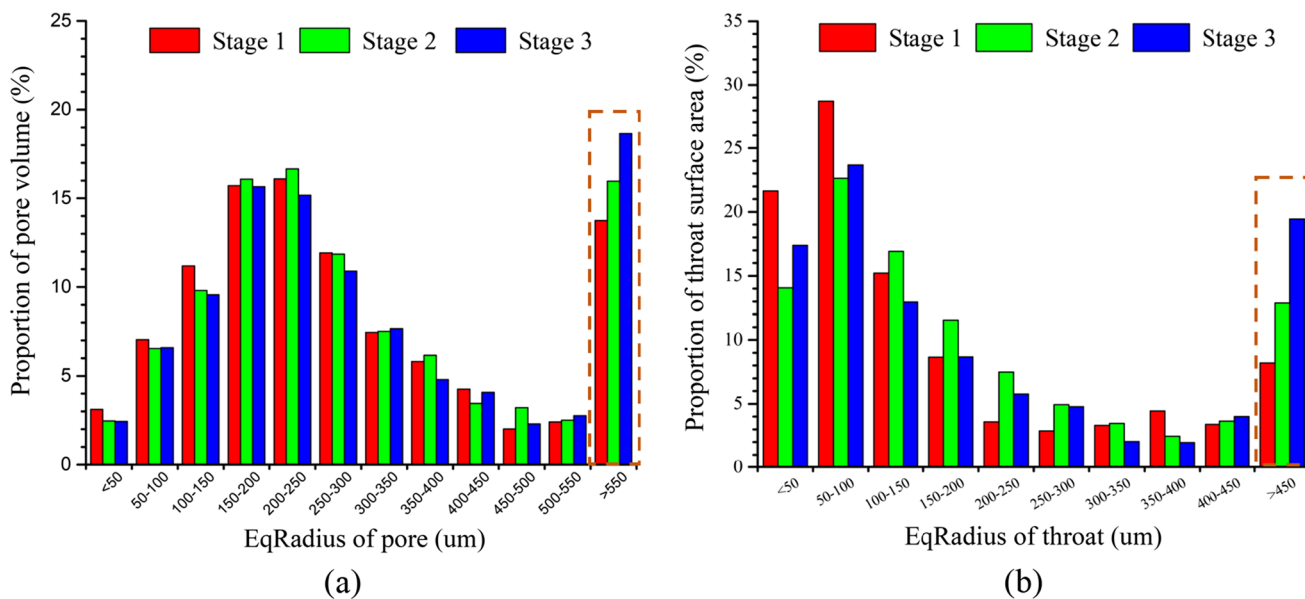


Fig. 21 Distribution of pore volume proportion and throat surface area proportion of Jinan red clay under three different stages of the whole experiment: **a** pore volume proportion and **b** throat surface area proportion

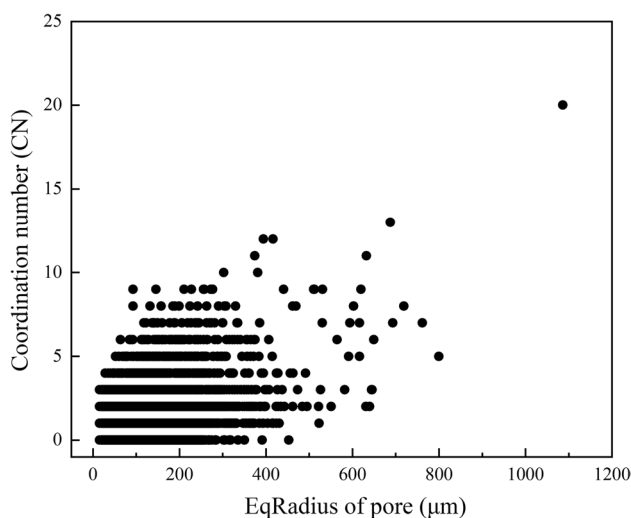


Fig. 22 Coordination number (CN) distribution versus pore EqRadius

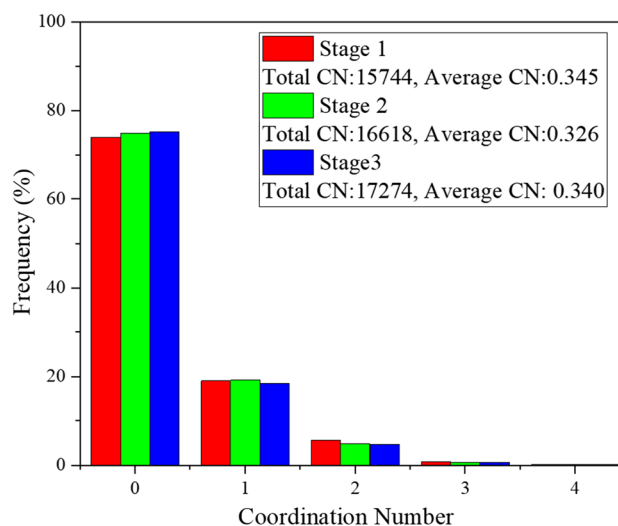


Fig. 23 Distribution of coordination number (CN) under three different stages of the whole experiment

drainage systems to solve the seepage problem of the excavation in Jinan red clay area.

Absolute permeability computation based on seepage experiment simulations

Absolute permeability, which appears in Darcy’s law as a constant coefficient, is defined as the measure of the ability of a porous material to transmit a single-phase fluid. In this study, the seepage experiment simulations were conducted based on the 3D pore structure of red clay using Avizo-Xlab Hydro module, and the absolute permeability of different Regions of

Interest (ROI) were calculated. The absolute permeability K (m^2) of soil is calculated by Eq. (3):

$$K = \frac{Q\mu L}{A\Delta P} \tag{3}$$

where Q (m^3/s) denotes the volumetric flow rate that goes through the porous media; μ (Pa s) is the dynamic viscosity of the flowing fluid, set as 0.001 Pa s, representing the viscosity coefficient of water at 20 degrees centigrade; L (m) is the length of the calculated sample, set as 0.005 m; A (m^2)

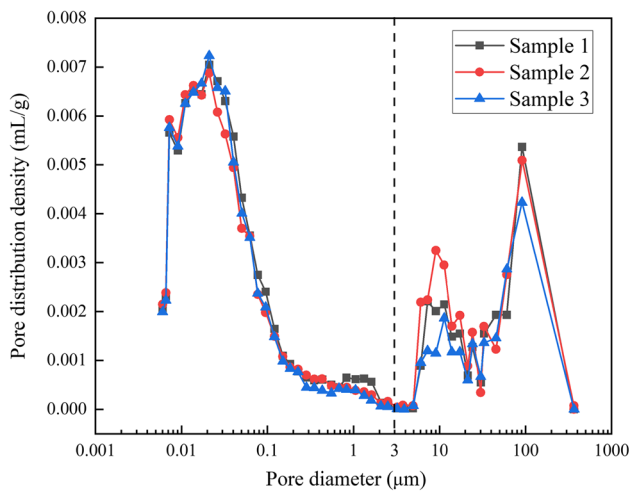


Fig. 24 MIP results of Jinan red clay

denotes the area of flow cross-section, set as 0.000025 m^2 ; ΔP is the pressure difference applied in the vertical direction of the sample, which is also set as 10 kPa.

The hydraulic conductivity $k(\text{m/s})$ in Darcy's law can be converted from the value of absolute permeability K according to Eq. (2).

The micro-scale flow is solved based on the Navier–Stokes equation. To make the calculation easier, a simplified Stokes' equation was used for the incompressible and Newtonian fluid in a steady and laminar flow manner (Eq. 4):

$$\begin{cases} \vec{\nabla} \cdot \vec{V} = 0 \\ \mu \nabla^2 \vec{V} - \vec{\nabla} P = 0 \end{cases} \quad (4)$$

where $\vec{\nabla}$ is the divergence operator; $\vec{\nabla}$ is the gradient operator; V is the velocity of the fluid; ∇^2 is the Laplacian operator; P is the pressure of the fluid in the fluid phase of the material.

Three different ROI with same size ($5000 \times 5000 \times 5000 \text{ μm}^3$) were extracted from the 3D pore structure of each intact Jinan red clay sample as shown in Fig. 25, where PF region represents the region with obvious preferential flow, and NPF region represents the area, where there is no obvious preferential flow.

The seepage simulation results of streamlines for different ROI of three intact samples are demonstrated in Fig. 26. It can be observed that the number and distribution density of streamlines in the PF regions are greater than the other two NPF regions for three samples. In addition, the seepage flow paths through the ROI box of the PF region are also more complete, with greater flow velocity. For NPF regions, the vast majority of the seepage streamlines are cut off halfway,

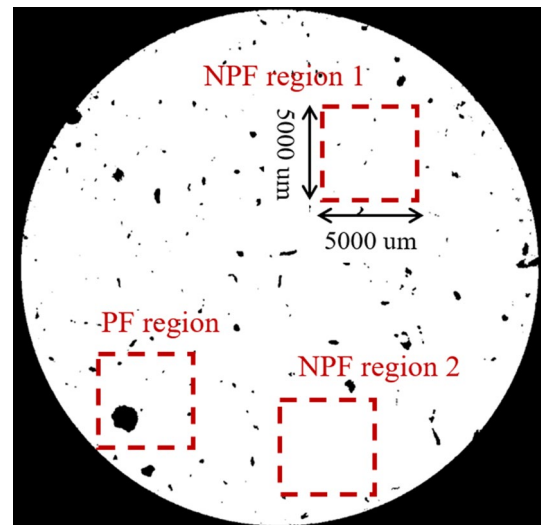


Fig. 25 Different ROI regions in horizontal cross sections of sample

especially for the NPF regions of T1 sample, the streamlines are almost invisible, indicating that there is almost no seepage in this area.

The results of absolute permeability $K(\text{μm}^2)$ and the corresponding hydraulic conductivity $k (\times 10^{-6} \text{ m/s})$ were presented in Table 3. The results calculated by seepage simulations show that the value of absolute permeability, as well as hydraulic conductivity of PF region is two orders of magnitude higher than that of NPF region. It can be noted that the calculated value of hydraulic conductivity is lower than that obtained from field pumping test ($1.4 \times 10^{-4} \text{ m/s}$) and laboratory seepage experiment ($7.51 \times 10^{-6} \text{ m/s}$), even for PF regions. This can be attributed to the fact that the preferential flow phenomenon is more obvious in the actual stratum, and the sizes of the ROI and the samples used in laboratory are relatively small. Hence, some connected pores are cut off in DOI or test samples, making it impossible to have a positive impact on permeability. The hydraulic conductivity obtained from laboratory seepage experiment is closer to that of PF region from seepage simulation, indicating the seepage characteristics of Jinan red clay are mainly dominated by the preferential flow region, which is consistent with the conclusion obtained from PNM in “Analysis of the micro-pore characteristics based on the establishment of Pore Network Model (PNM)”.

The maximum pore EqRadius, pore volume content, and pore connectivity of each ROI were also listed, where the pore volume content is the ratio of pore volume to the volume of ROI, the pore connectivity is the ratio of connected pore volume to the total pore volume. It can be known that the pore volume content of different ROI is similar, indicating the pore volume content has little influence on the soil permeability. The high hydraulic

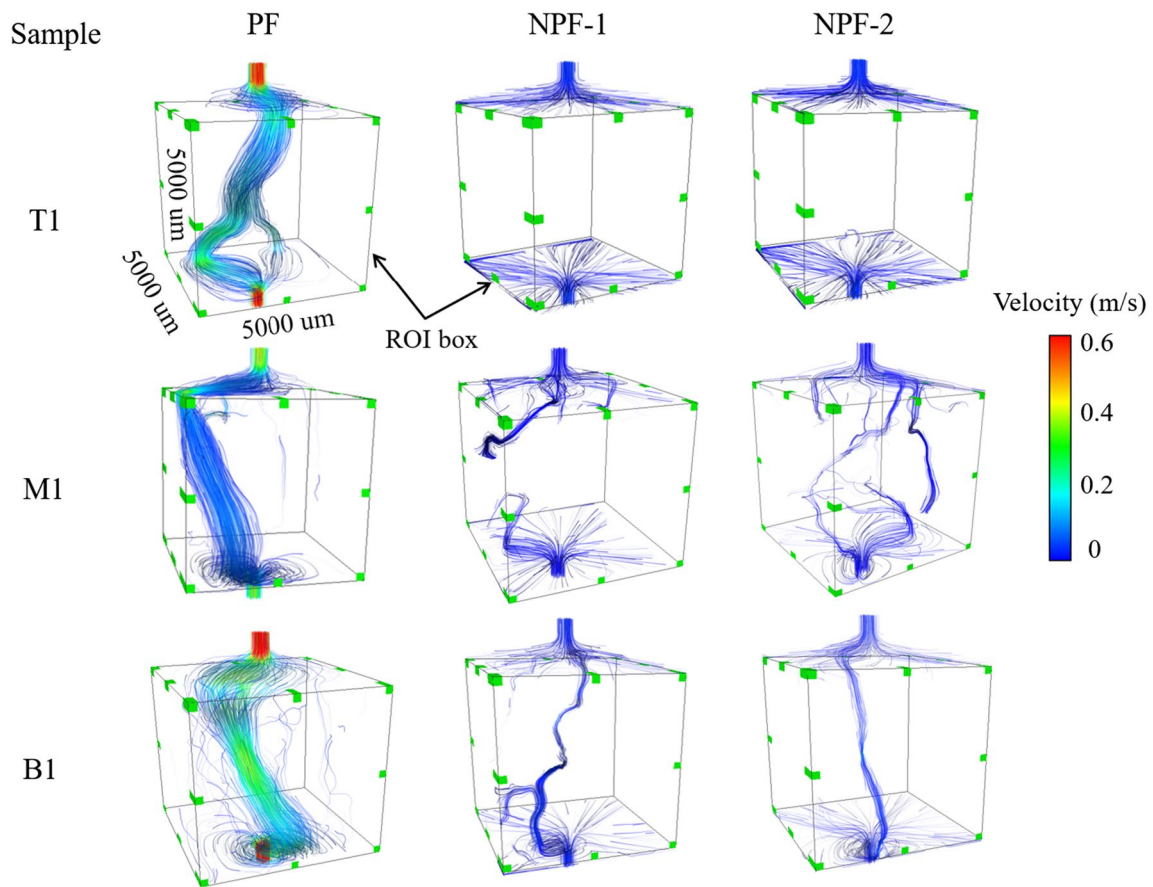


Fig. 26 Seepage simulation results of streamlines for different ROI of samples

Table 3 Calculated results of seepage experiment simulation

Sample	ROI	Maximum pore EqRadius (μm)	Pore volume content (ϕ /%)	Pore connectivity (β /%)	Absolute permeability (μm ²)	Hydraulic conductivity ($\times 10^{-6}$ m/s)
T1	PF	1321	14.6	46.8	289.11	2.83
	NPF-1	32	10.8	1.2	0.16	0.0016
	NPF-2	40	12.3	2.7	0.17	0.0017
M1	PF	1061	13.3	38.7	146.01	1.43
	NPF-1	245	13.8	9.8	5.73	0.06
	NPF-2	368	12.7	13.2	9.30	0.09
B1	PF	1645	15.9	59.8	589.11	5.77
	NPF-1	434	10.6	17.5	11.58	0.11
	NPF-2	458	10.8	16.8	11.84	0.11

conductivity in the PF region is due to existence of large pores with good connectivity. Figure 27 shows the relation between absolute permeability and different pore parameters. It is found that the absolute permeability increases with the maximum pore EqRadius and pore connectivity. The seepage characteristics for Jinan red clay is more

complicated, which is less related to porosity, but closely related to the pore morphology, connectivity, and other factors. The seepage simulation results show that the maximum pore EqRadius and pore connectivity have important influence on seepage characteristics, which is consistent with the conclusion obtained from seepage experiment.

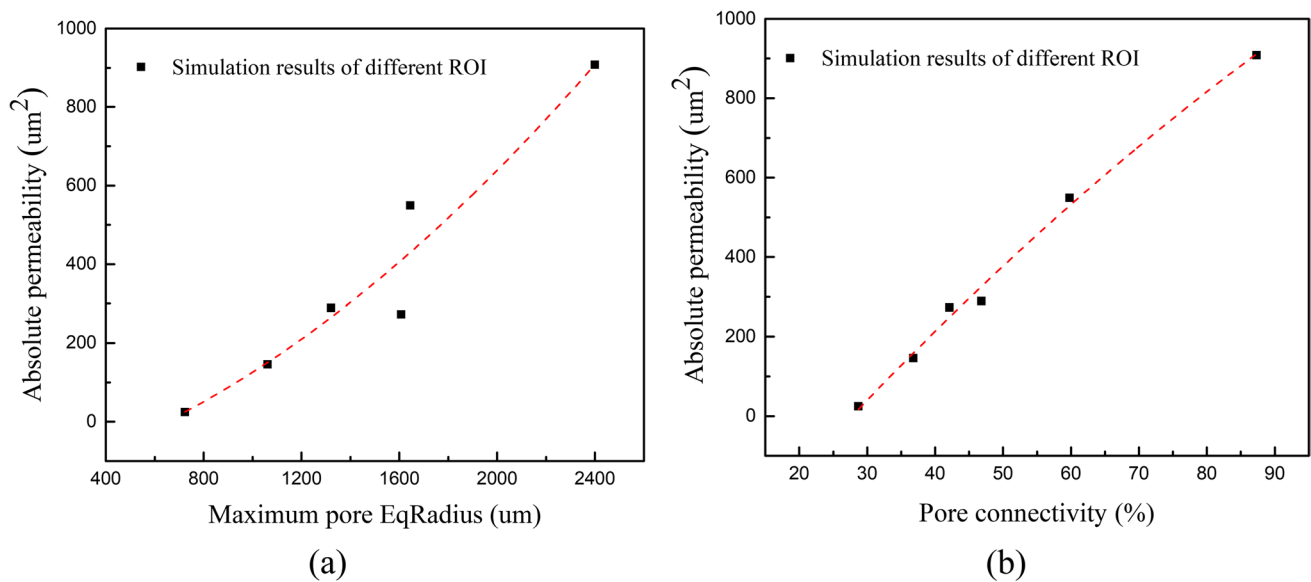


Fig. 27 Relation curve between absolute permeability and pore parameters: **a** maximum pore EqRadius and **b** pore connectivity

Conclusions

This paper proposes a new approach to identify the water flow and analyse the micro-pore characteristics of clay combining seepage experiment with X-ray micro-tomography system. The 3D pore space of the sample under different seepage stages was quantitatively identified and characterized by some geometrical parameters based on PNM, such as pore size distribution, throat size distribution. The seepage experiment simulations were conducted and the pore parameters affecting the soil permeability were analysed. The main conclusions obtained in this study are as follows:

1. The unique pore structure and soil properties lead to the strong vertical permeability of Jinan red clay. The pore structure of Jinan red clay is mainly vertically developed with macropore channel existing, which is caused by the long-term vertical seepage and the decaying roots during sedimentation. The seepage characteristics of Jinan red clay are mainly dominated by the preferential flow region. The preferential flow phenomenon is more obvious in the actual stratum, which leads to a higher hydraulic conductivity obtained from field pumping test compared with the results obtained from laboratory seepage experiments and seepage simulations.
2. The equivalent Pore Network Model (PNM) representing pore structure of Jinan red clay was established, and the micro-pore parameters were quantified. The PNM results show that Jinan red clay is mainly composed of isolated small pores, and the macropores more likely have a good connectivity with greater CN. The macropore channel has major influence on the seepage

characteristics of red clay. The pore throat length and CN are almost unchanged, implying the washed-out particles mainly come from the pore walls, while the clay matrix stays intact.

3. The seepage experiment simulations were conducted based on the 3D pore structure of Jinan clay, and the absolute permeability of different ROI were calculated. The results show that the value of absolute permeability of PF region is two orders of magnitude higher than that of NPF region. The maximum pore EqRadius and pore connectivity have important influence on seepage characteristics of Jinan red clay, but the correlation between porosity is small.
4. The approach combined with soil seepage experiment and micro-CT scanning can be used to study the microscopic seepage characteristics of a wide range of soil types. Macro-pores in the soil which form preferential flow channels have a significant influence on soil seepage characteristics, even though they are not account for a high porosity. The mineral composition and content of soil influence the possibility of expansion or contraction of seepage channel. The factors such as: existence of macro-pore, pore connectivity play a positive role on soil seepage characteristics.

Acknowledgements The financial support from the National Natural Science Foundation of China (NSFC Grant Nos. 42207186, 42072317), and Natural Science Foundation of Shandong Province (Grant No. ZR2020ME258) are gratefully acknowledged.

Availability of data and materials The raw data required to produce the above findings cannot be shared at this time due to time limitations.

Declarations

Conflict of interest We declare that we have no conflicts of interest to this work. We declare that we do not have any commercial or associative interest that represents a conflict of interest in connection with the work submitted.

References

- Alonso EE, Romero E, Hoffmann C (2011) Hydromechanical behaviour of compacted granular expansive mixtures: experimental and constitutive study. *Geotechnique* 61:329–344. <https://doi.org/10.1680/geot.2011.61.4.329>
- Boynton SS, Daniel DE (1985) Hydraulic conductivity tests on compacted clay. *J Geotech Eng* 111(4):465–478. [https://doi.org/10.1061/\(ASCE\)0733-9410\(1985\)111:4\(465\)](https://doi.org/10.1061/(ASCE)0733-9410(1985)111:4(465))
- Chang DS, Zhang LM (2013) Critical hydraulic gradients of internal erosion under complex stress states. *J Geotech Geoenviron Eng* 139(9):1454–1467. [https://doi.org/10.1061/\(ASCE\)GT.1943-5606.0000871](https://doi.org/10.1061/(ASCE)GT.1943-5606.0000871)
- Chen Y, Ma G, Zhou W, Wei D, Zhao Q, Zou Y (2021) An enhanced tool for probing the microscopic behavior of granular materials based on X-ray micro-CT and FDEM. *Comput Geotech* 132:103974. <https://doi.org/10.1016/j.compgeo.2020.103974>
- Chen Z, Liu H, Zhu C, Ma S, Hang Y, Luo W (2022) Seepage characteristics and influencing factors of weakly consolidated rocks in triaxial compression test under mining-induced stress path. *Minerals* 12(12):1536
- Della VG, Musso G (2016) Some remarks on single-and double-porosity modeling of coupled chemo-hydro-mechanical processes in clays. *Soils Found* 56(5):779–789
- Ghadr S, Assadi-Langroudi A (2018) Structure-based hydro-mechanical properties of sand-bentonite composites. *Eng Geol* 235:53–63
- Huang C, Laften JM (1996) Seepage and soil erosion for a clay loam soil. *Soil Sci Soc Am J* 60:408–416. <https://doi.org/10.2136/sssaj1996.03615995006000020011x>
- Jefferson I, Smalley I (1995) Six definable particle types in engineering soils and their participation in collapse events: proposals and discussions. *Genesis and properties of collapsible soils*. Springer, pp 19–31
- Koestel J, Larsbo M (2014) Imaging and quantification of preferential solute transport in soil macropores. *Water Resour Res* 50:4357–4378
- Larsbo M, Koestel J, Jarvis N (2014) Relations between macropore network characteristics and the degree of preferential solute transport. *Hydrol Earth Syst Sci* 18(12):5255–5269
- Liu HH, Birkholzer J (2012) On the relationship between water flux and hydraulic gradient for unsaturated and saturated clay. *J Hydrol* 475:242–247
- Liu Y, Yin ZY, Wang L, Hong Y (2021) A coupled CFD–DEM investigation of internal erosion considering suspension flow. *Can Geotech J* 58(9):1411–1425
- Luo L, Lin H, Schmidt J (2010) Quantitative relationships between soil macropore characteristics and preferential flow and transport. *Soil Sci Soc Am J* 74(6):1929–1937
- Lyu Q, Wu H, Li X (2021) A 3D model reflecting the dynamic generating process of pore networks for geological porous media. *Comput Geotech* 140:104444. <https://doi.org/10.1016/j.compgeo.2021.104444>
- Miller RJ, Low PF (1963) Threshold gradient for water flow in clay systems. *Soil Sci Soc Am J* 27:605–609
- Naveed M, Moldrup P, Arthur E, Wildenschild D, Eden M, Lamandé M, Vogel HJ, Jonge LW (2013) Revealing soil structure and functional macroporosity along a clay gradient using x-ray computed tomography. *Soil Sci Soc Am J* 77(2):403–411. <https://doi.org/10.2136/sssaj2012.0134>
- Nguyen XP, Cui YJ, Tang AM, Deng YF, Li XL, Wouters L (2013) Effects of pore water chemical composition on the hydro-mechanical behavior of natural stiff clays. *Eng Geol* 166:52–64. <https://doi.org/10.1016/j.enggeo.2013.08.009>
- Nguyen CD, Benahmed N, Andò E, Sibille L, Philippe P (2019) Experimental investigation of microstructural changes in soils eroded by suffusion using X-ray tomography. *Acta Geotech* 14(3):749–765
- Reddi LN, Lee IM, Bonala MV (2000) Comparison of internal and surface erosion using flow pump tests on a sand-kaolinite mixture. *Geotech Test J* 23(1):116–122
- Rolfe PF, Aylmore LAG (1977) Water and salt flow through compacted clays: I. Permeability of compacted illite and montmorillonite. *Soil Sci Soc Am J* 41(3):489–495. <https://doi.org/10.2136/sssaj1977.03615995004100030011x>
- Sakellariou A, Sawkins TJ, Senden TJ, Limaye A (2004) X-ray tomography for mesoscale physics applications. *Phys A Stat Mech Its Appl* 339(1–2):152–158. <https://doi.org/10.1016/j.physa.2004.03.055>
- Taylor HF, O’Sullivan C, Sim WW (2015) A new method to identify void constrictions in micro-CT images of sand. *Comput Geotech* 69:279–290. <https://doi.org/10.1016/j.compgeo.2015.05.012>
- Thermo Scientific Avizo Software User’s Guide (2015) FEI Visualization Sciences Group. Avizo 9.0.1
- Wang K, Zhang S, DelgadoTéllez R, Wei F (2019) A new slope unit extraction method for regional landslide analysis based on morphological image analysis. *Bull Eng Geol Environ* 78:4139–4151. <https://doi.org/10.1007/s10064-018-1389-0>
- Wei T, Fan W, Yuan W, Wei YN, Yu B (2019) Three-dimensional pore network characterization of loess and paleosol stratigraphy from South Jingyang Plateau, China. *Environ Earth Sci* 78(11):1–15
- Yu B, Fan W, Fan JH, Dijkstra TA, Wei YN, Wei TT (2020) X-ray micro-computed tomography (μ -CT) for 3D characterization of particle kinematics representing water-induced loess micro-fabric collapse. *Eng Geol* 279:105895. <https://doi.org/10.1016/j.enggeo.2020.105895>
- Zhang Z, Sui W, Wang K, Tang G, Li X (2018) Changes in particle size composition under seepage conditions of reclaimed soil in Xinjiang, China. *Processes* 6(10):201. <https://doi.org/10.3390/pr6100201>
- Zhao Y, Zhu G, Liu S, Wang Y, Zhang C (2019) Effects of pore structure on stress-dependent fluid flow in synthetic porous rocks using microfocus x-ray computed tomography. *Transp Porous Media* 128:653–675. <https://doi.org/10.1007/s11242-019-01264-4>
- Zhou XP, Xiao N (2019) Analysis of fracture properties of three-dimensional reconstructed rock model using hierarchical-fractal annealing algorithm. *Eng Geol* 256:39–56. <https://doi.org/10.1016/j.enggeo.2019.04.017>
- Zuo L, Xu L, Baudet BA, Gao C, Huang C (2020) The structure degradation of a silty loess induced by long-term water seepage. *Eng Geol* 272:105634. <https://doi.org/10.1016/j.enggeo.2020.105634>

Publisher’s Note Springer Nature remains neutral with regard to jurisdictional claims in published maps and institutional affiliations.

Springer Nature or its licensor (e.g. a society or other partner) holds exclusive rights to this article under a publishing agreement with the author(s) or other rightsholder(s); author self-archiving of the accepted manuscript version of this article is solely governed by the terms of such publishing agreement and applicable law.